Physical insights into the sonochemical degradation of recalcitrant organic pollutants with cavitation bubble dynamics

ARTICLE *in* ULTRASONICS SONOCHEMISTRY · MARCH 2009

Impact Factor: 4.32 · DOI: 10.1016/j.ultsonch.2009.02.009 · Source: PubMed

Ultrasonics Sonochemistry 16 (2009) 769–781

Contents lists available at ScienceDirect

Ultrasonics Sonochemistry

journal homepage: www.elsevier.com/locate/ultsonch

Physical insights into the sonochemical degradation of recalcitrant organic pollutants with cavitation bubble dynamics

Thirugnanasambandam Sivasankar, Vijayanand S. Moholkar *

Department of Chemical Engineering, Indian Institute of Technology Guwahati, Guwahati 781 039, Assam, India

ARTICLE INFO

Article history:
Received 19 December 2008
Received in revised form 6 February 2009
Accepted 16 February 2009
Available online 27 February 2009

Keywords:
Sonochemistry
Cavitation
Bubble dynamics
Wastewater treatment

ABSTRACT

This paper tries to discern the mechanistic features of sonochemical degradation of recalcitrant organic pollutants using five model compounds, viz. phenol (Ph), chlorobenzene (CB), nitrobenzene (NB), p-nitrophenol (PNP) and 2,4-dichlorophenol (2,4-DCP). The sonochemical degradation of the pollutant can occur in three distinct pathways: hydroxylation by ·OH radicals produced from cavitation bubbles (either in the bubble–bulk interfacial region or in the bulk liquid medium), thermal decomposition in cavitation bubble and thermal decomposition at the bubble–liquid interfacial region. With the methodology of coupling experiments under different conditions (which alter the nature of the cavitation phenomena in the bulk liquid medium) with the simulations of radial motion of cavitation bubbles, we have tried to discern the relative contribution of each of the above pathway to overall degradation of the pollutant. Moreover, we have also tried to correlate the predominant degradation mechanism to the physico-chemical properties of the pollutant. The contribution of secondary factors such as probability of radical–pollutant interaction and extent of radical scavenging (or conservation) in the medium has also been identified. Simultaneous analysis of the trends in degradation with different experimental techniques and simulation results reveals interesting mechanistic features of sonochemical degradation of the model pollutants. The physical properties that determine the predominant degradation pathway are vapor pressure, solubility and hydrophobicity. Degradation of Ph occurs mainly by hydroxylation in bulk medium; degradation of CB occurs via thermal decomposition inside the bubble, degradation of PNP occurs via pyrolytic decomposition at bubble interface, while hydroxylation at bubble interface contributes to degradation of NB and 2,4-DCP.

1. Introduction

Wastewater discharge from chemical and process industries often contain numerous aromatic compounds that are refractory to microorganisms. These compounds cannot be completely degraded by the conventional biological wastewater treatment methods. Alternate technologies popularly known as Advanced Oxidation Processes (AOPs) have been extensively explored for effective degradation of these compounds for the past few decades. The AOPs are characterized by production of ·OH (hydroxyl) radical as primary oxidant. The ·OH radicals are extremely reactive species and are powerful oxidizing agent with an oxidation potential of 2.33 V. The typical rate constant for the reaction of ·OH radicals with organic compounds ranges between 10^6–10^9 mol^{-1} s^{-1} [1].

Sonochemical oxidation (or Sonolysis) has been investigated as a viable AOP for the destruction of aromatic pollutants in the past one and half decade [2–5]. In this technique, the free radicals are generated through transient collapse of cavitation bubbles driven by an ultrasound wave. The possible sources of nuclei for the cavitation bubbles are tiny gas pockets trapped in the crevices of solid boundaries (such as the reactor wall) or tiny bubbles already suspended in the medium. Under the influence of pressure variation in bulk liquid due to passage of the acoustic wave, these nuclei grow into cavitation bubbles with the evaporation of water at gas–liquid interface. The water vapor thus entered in the bubble condenses at the gas–liquid interface during the compression phase. At the final moments of bubble collapse, the dynamics of the bubble motion becomes extremely fast and not all of the water vapor that has evaporated in the bubble can condense. This causes entrapment of vapor molecules in the bubble [6–8]. The entrapped molecules are subjected to extremes of temperature and pressure (of the order of 5000 K and 500 bar [9]) generated during transient and adiabatic collapse of the bubble and undergo dissociation generating radicals [10,11]. With fragmentation of the bubble during collapse, these radicals are released into the bulk liquid medium where they induce various chemical reactions; an example of which is the oxidation of the pollutant molecules present in the medium.

The two major pathways or mechanisms for the sonolytic degradation of a pollutant are thermal decomposition of the pollutant

* Corresponding author. Tel.: +91 361 258 2258; fax: +91 361 269 0762.
E-mail address: vmoholkar@iitg.ac.in (V.S. Moholkar).

1350-4177/$ - see front matter © 2009 Elsevier B.V. All rights reserved.
doi:10.1016/j.ultsonch.2009.02.009

molecules entrapped inside the bubble [12,13], and secondly, the attack of O·, ·OH and HO_2 radicals produced by the cavitation bubble (out of dissociation of water molecules during transient collapse) on the pollutant molecules in the bulk solution leading to hydroxylated products that are further degraded to the final products, i.e. CO_2 and H_2O [6]. Hua et al. [14] have proposed a third possible mechanism for the sonochemical degradation of organic pollutants, which is hydrolysis of the organic pollutants in the transient supercritical water packets formed in the close vicinity of cavitation bubble during transient collapse. Out of these pathways, the major pathway contributing to the overall degradation depends on the nature and physico-chemical properties of the organic compound. An analysis of the degradation products of the pollutant provides a preliminary insight into the dominant chemical mechanism for the degradation. One can conclude from the above discussion that the radial motion of the cavitation bubble driven by ultrasound wave (or the bubble dynamics) is the basic physical phenomenon underlying sonochemical degradation of pollutants.

In this paper, we have addressed the issue of establishing a general framework for the determination of the physical mechanism of the sonochemical degradation of organic pollutants. To achieve this, we have adopted a twofold approach, i.e. correlation of the experimental results under different conditions to the simulations of the radial motion of cavitation bubbles and the physico-chemical properties of the pollutants. We have chosen five model pollutants, viz. phenol (Ph), chlorobenzene (CB), nitrobenzene (NB), p-nitrophenol (PNP) and 2,4-dichlorophenol (2,4-DCP) for our study. These are very common pollutants found in industrial wastewater. Various experimental techniques adopted in this study cause variation in the nature of the cavitation phenomenon occurring in the medium. The trends in the degradation observed with these experimental conditions have been correlated to the simulations of the radial motion of cavitation bubbles. For the simulations, we use a mathematical model that takes into account essential physics and chemistry of the cavitation bubbles. This model is able to predict the amount of water vapor and pollutant evaporated and entrapped into the bubble, and the temperature and pressure peaks attained during transient collapse. Using this data, we can estimate the number of ·OH and other radicals generated per cavitation bubble and released into the bulk medium with fragmentation of the bubble at transient collapse. As outlined in the subsequent sections, a concurrent analysis of the simulations and experimental results vis-à-vis the physico-chemical properties of the pollutants helps us to establish the predominant physical mechanism of the sonochemical degradation of the pollutant.

2. Experimental

Materials: The following reagents were used in this study: phenol (Merck, Grade: Synthesis), iron(II) sulphate heptahydrate (Merck, Grade: Purified), chlorobenzene (Merck, Grade: GR), sodium chloride (Merck, Grade: Pure), nitrobenzene (Merck, Grade: Synthesis), *p*-nitrophenol (Loba Chemicals, Grade: Pure), sodium hydroxide (Merck, Grade: Purified pellets), 2,4-dichlorophenol (Loba Chemie, Grade: Synthesis), acetonitrile (Merck, Grade: HPLC) and water (Merck, Grade: HPLC). All reagents were used as received. Elix water from Millipore® purification unit (Model: Elix 3) was used for the preparation of the aqueous solutions of pollutants. Four gases, viz. oxygen, argon, nitrogen and air (99.99% purity) were used for sparging the reaction solution. The initial concentrations of the aqueous solutions of different pollutants are: Ph – 50 and 100 ppm, CB – 50 and 100 ppm, NB – 100 ppm, PNP – 10 ppm and 2,4-DCP – 100 ppm. These concentrations are typical of those appearing in industrial wastewater.

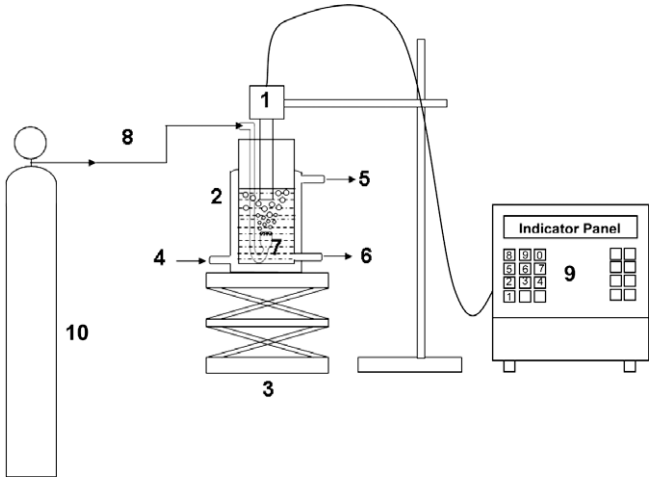

Fig. 1. Schematic of experimental set-up [*Legends:* 1 – ultrasound horn; 2 – jacketed glass reactor; 3 – laboratory jack; 4 – cooling water inlet; 5 – cooling water outlet; 6 – sample port; 7 – aerator; 8 – gas inlet; 9 – control unit of ultrasonic processor; 10 – gas cylinder].

Experimental set-up: Sonication of the aqueous solution of pollutant was carried out in a jacketed glass reactor (volume 250 mL) using a probe type ultrasonic processor operating at a frequency of 20 kHz (Sonics and Materials Inc., Model VCX 500). A schematic of the experimental set-up is shown in Fig. 1. The processor had a sonicator probe with a tip diameter of 13 mm. The processor had variable power output control, which was set at 20% during experiments, resulting in net consumption of 100 W power. In addition, the processor had facility of automatic frequency tuning and amplitude compensation. Temperature of the reaction medium is a critical factor influencing the cavitation phenomena. Hence, the temperature of the reaction medium during sonication was controlled by circulating cooling water through the jacket of the reactor. The actual value of the ultrasound intensity in the medium was determined using calorimetry [15]. For a power output of 100 W, the ultrasound probe produced an acoustic wave with 150 kPa amplitude. For bubbling of different gases through the reaction medium during sonication, a glass sparger was used. This sparger distributed the gas entering into the reaction medium through a porous silica filter of pore size ~40 μm. The sparger was so positioned that the porous silica filter exactly faces the bottom of the ultrasound probe. This feature helps uniform distribution of gas bubbles forming cavitation nuclei in the solution. The distance between ultrasound probe tip and silica filter was fixed at 20 mm. The flow rate of the sparge gases were maintained at 5 L h^{-1} with the help of a rotameter.

Experimental procedure: Synthetically prepared solutions of pollutants (with different initial concentrations as outlined earlier) were sonicated for a total reaction time of 90 min. Sonication was done with 15 min on and 5 min off cycle in order to reduce the significant temperature rise in the reaction medium. The temperature of the reaction medium was monitored continuously using a digital thermometer. The rise in temperature of the medium during 90 min of sonication was only 2 °C. Various techniques or experimental conditions applied during sonication of the solution of the pollutant are as follows:

(1) Variation in the initial concentration of the pollutant.
(2) Variation in the saturation level (or dissolved gas content) of the solution.
(3) Addition of salt (NaCl) to the solution of pollutant (either saturated or unsaturated) in concentration of 4% w/v.

(4) Sparging of monatomic or diatomic gases such as Ar, N_2, O_2 and air through the pollutant solution during sonication.
(5) Addition of $FeSO_4 \cdot 7H_2O$ to the pollutant solution (either saturated or unsaturated) in concentration of 0.5 mM.

We would like to categorically mention that not all of the above techniques were applied to all five pollutants. For each pollutant, only those techniques were applied, which were sufficient to establish the dominant physical mechanism of the sonochemical degradation.

Variation in dissolved gas content: For experiments with unsaturated (or degassed) medium, the dissolved gas content of the liquid medium was reduced by vacuumization. A vacuum of 86.65 kPa was applied for a time period of 30 min with intermittent stirring using a vacuum pump (Riviera, Model: TID-25-S). This procedure reduced the dissolved oxygen (DO) content of the medium to 2.7 ppm, which was measured using a DO meter (Make: Consort, Model: C863). The dissolved gas content, however, rises during sonication due to induction of air. In order to maintain the unsaturation of the medium, the DO content of the medium was continuously monitored during off cycle of sonication. When the DO content increased above 4 ppm, the reaction solution was re-vacuumized to restore the unsaturation level to 2.7 ppm of DO. With this procedure, the average DO content of the solution in the experiments with unsaturated medium was ~3 ppm.

Analytical procedure: The extent of sonochemical degradation of Ph, NB, CB and DCP was monitored with HPLC (Perkin–Elmer, Model: Series 200). A C18 column (250 mm × 4.5 mm) with the packing of 5 μm size silica particles was used. The mobile phase was a mixture of acetonitrile and water (80:20). The eluent mixture was passed at a constant flow rate of 0.75 mL min^{-1} and the sample injection volume was 20 μL. The UV detector wavelengths for various pollutants were as follows: Ph and DCP – 275 nm, CB – 205 nm, NB – 254 nm. Sonochemical degradation of PNP was analyzed using UV–Vis spectrophotometer (Perkin–Elmer, Model: Lamda 35). Before analysis, the sample was made alkaline (with pH adjusted to 11) by addition of 0.5 N NaOH to solution. The peak absorbance spectrum occurred at 355 nm. We categorically state that we have not made an analysis of the intermediate products of degradation, as these have been extensively studied in previous literature as follows:

Ph: Hydroquinone, catechol, p- and o-benzoquinone, muconic acid, maleic acid and succinic acid [16–20].

CB: Methane, acetylene, butenyne, butadiyne, benzene, chlorophenols and phenylacetylene [21–24].

NB: 4-Nitrophenol, 3-nitrophenol and 4-nitrocatechol [25,26].

PNP: Nitrites (NO_2^-) and nitrates (NO_3^-), short chain carboxylic acids, formic acid (or formate), acetic acid (or acetates), oxalic acid (or oxalate), 4-nitrocatechol, hydroquinone and benzoquinone [27,28].

2,4-DCP: 2-chlorophenol, 4-chlorophenol and phenol [29–31].

We have only monitored the rate of disappearance of original pollutant and the analysis has been made on that basis. We justify our approach as follows: The aim of this study is to discern the physical (and not chemical) mechanism of the degradation of organic pollutants. Experiments done in this study vary the characteristics of the cavitation phenomenon in the medium, which are not likely to affect the degradation chemistry. Therefore, the intermediates, final products and kinetics of the sonochemical degradation of the pollutants is expected to be same in the present study as previous literature, as we make only physical changes to the conditions of the experiments which have been done earlier; with chemical conditions or protocol remaining the same.

3. Mathematical model for cavitation bubble dynamics

The overall sonochemical degradation of the pollutant is a result of collective oscillations and collapse of millions of cavitation bubbles, with strong interaction among them. No mathematical model has been developed so far, which would take into account a multi-bubble system along with other physical phenomena associated with it such as bubble–bubble coalescence, clustering and rectified diffusion. Another important parameter that influences in the overall intensity of cavitation in the system, and hence, the extent of sonochemical degradation is the number density of bubbles. No experimental method has been developed yet, which can provide even an order of magnitude estimate of this parameter. In view of these limitations, we choose single bubble model for our analysis. Although the single bubble analysis does not address entire physics of the sonochemical system, it does provide a qualitative physical insight into the problem as demonstrated by others [15,32–35]. Quantitative predictions of the degradation kinetics of pollutants cannot be made with the single bubble model. However, the present study is aimed at gaining a qualitative physical insight into the sonochemical degradation of various organic pollutants. For meeting this objective, single bubble analysis is sufficient.

Modeling of the radial motion of cavitation bubbles and the production of various chemical species out of it has been a subject of intensive investigation in the past two decades, with different authors addressing the problem with different perspective [6–8,33,36–41]. In our previous papers, we have presented a review of the literature in this area [15,42], and we refer the readers to these papers for greater information about previous investigations. The most general treatment of the problem of water vapor transport across a cavitation bubble during large amplitude nonlinear motion was presented by Storey and Szeri [8]. The principal result of analysis of Storey and Szeri [8] (on the basis of relative time scales of various phenomena such as water vapor diffusion, condensation and radial motion of bubbles) was that water vapor transport in the bubble is a diffusion-limited (and not condensation limited) process. In view of these conclusions, Toegel et al. [41] developed a simplified model using boundary layer approximation, which is used in the present study. This model has been described extensively in our earlier papers [15,42,43], and therefore, we reproduce here only the essential equations and thermodynamic data of this model in Tables 1A and 1B. For greater details on other aspects of the model, we refer the reader to our previous papers [15,42]. The main components of the model for radial motion of cavitation bubble are:

(1) Equation for the radial motion of the bubble [44–46].
(2) Equation for the diffusive flux of water vapor and pollutant vapor across bubble wall. In these equations, the binary diffusion coefficients for water vapor and pollutant vapor are determined using Chapman–Enskog theory using Lennard–Jones 12-6 potential at the bulk temperature of the liquid medium [47–49]. The overall diffusion coefficient in ternary mixture (e.g. N_2–O_2–H_2O in case of air bubbles) or quaternary mixture (e.g. N_2–O_2–H_2O–CB, where pollutant also vaporizes into the bubble) has been determined using Blanc's law [49]. The diffusive penetration depth has been estimated using dimensional analysis.
(3) Equation for heat conduction through bubble wall. The thermal conductivity of the bubble content (mixture of gas and water vapor and pollutant vapor, in case of volatile pollutants) is determined using Chapman–Enskog theory using Lennard–Jones 12-6 potential at the bulk temperature of the liquid medium [47–49]. In this case, the thermal penetration depth is estimated using dimensional analysis.

Table 1A
Summarization of the bubble dynamics formulation.

Variable	Equation	Boundary Condition
1. Radius of the bubble (R) 2. Bubble wall velocity (dR/dt)	$\left(1-\frac{dR/dt}{c}\right)R\frac{d^2R}{dt^2}+\frac{3}{2}\left(1-\frac{dR/dt}{3c}\right)\left(\frac{dR}{dt}\right)^2=\frac{1}{\rho_L}\left(1+\frac{dR/dt}{c}\right)(P_i-P_t)+\frac{R}{\rho_L c}\frac{dP_i}{dt}-4\nu\frac{dR/dt}{R}-\frac{2\sigma}{\rho_L R}$ Internal pressure in the bubble: $P_i=\frac{N_{tot}(t)kT}{[4\pi(R^3(t)-h^3)/3]}$ Pressure in bulk liquid medium: $P_t=P_0-P_A\sin(2\pi ft)$	At $t=0$, $R=R_o$ and $dR/dt=0$.
3. Number of water molecules in the bubble (N_w) 4. Number of pollutant molecules in the bubble (N_p)	$\frac{dN_w}{dt}=4\pi R^2D_w\frac{\partial C_w}{\partial r}\Big\vert_{r=R}\approx 4\pi R^2D_w\left(\frac{C_{wR}-C_w}{l_{diff,w}}\right)$ $\frac{dN_p}{dt}=4\pi R^2D_p\frac{\partial C_p}{\partial r}\Big\vert_{r=R}\approx 4\pi R^2D_p\left(\frac{C_{pR}-C_p}{l_{diff,p}}\right)$ Instantaneous diffusive penetration depths: $l_{diff,w}=\min\left(\sqrt{\frac{RD_w}{\vert dR/dt\vert}},\frac{R}{\pi}\right);\ l_{diff,p}=\min\left(\sqrt{\frac{RD_p}{\vert dR/dt\vert}},\frac{R}{\pi}\right)$	At $t=0$, $N_w=0$ and $N_p=0$
5. Heat transfer through bubble (Q)	$\frac{dQ}{dt}=4\pi R^2\lambda\frac{\partial T}{\partial r}\Big\vert_{r=R}\approx 4\pi R^2\lambda\left(\frac{T_0-T}{l_{th}}\right)$ Thermal diffusion length: $l_{th}=\min\left(\sqrt{\frac{R\kappa}{\vert dR/dt\vert}},\frac{R}{\pi}\right)$	At $t=0$, $Q=0$
6. Temperature of the bubble (T)	$C_{V,mix}dT/dt=dQ/dt-P_idV+(h_w-U_w)dN_w/dt$ Mixture heat capacity: $C_{V,mix}=\sum C_{V,i}N_i$ Molecular properties of water: Enthalpy: $h_w=4kT_o$ Internal energy: $U_w=N_wkT\left(3+\sum_{i=1}^{3}\frac{\theta_i/T}{\exp(\theta_i/T)-1}\right)$ Heat capacity (Ar): $C_V=3kN_{Ar}/2$ Heat capacity of other species ($i=N_2/O_2/H_2O$): $C_{V,i}=N_ik(f_i/2+\sum((\theta_i/T)^2\exp(\theta_i/T)/(\exp(\theta_i/T)-1)^2))$	At $t=0$, $T=T_o$

(4) Overall energy balance treating the cavitation bubble as an open system.

This model ignores the diffusion of gases across bubble wall (or the rectified diffusion) as the time scale for the diffusion of gases (which is of the order of few milliseconds) is much higher than the time scale for the radial motion of bubble (which is of the order of few microseconds) [50]. Moreover, the evaporation of the pollutant molecules in the bubble is also ignored for Ph, NB, PNP and 2,4-DCP as the partial pressure of these pollutant at the bubble–bulk interface (calculated as the product of mole fraction of the pollutant and the vapor pressure at the temperature of the experiment) is very small (<10 Pa). For CB, however, the vaporization of the pollutant molecule in the bubble has been taken into account.

Table 1B
Thermodynamic properties of various species.*

Species	Degrees of freedom (translational + rotational) (f_i)	Lennard–Jones force constants		Characteristic vibrational temperatures θ (K)
		σ (10^{-10} m)	ε/k (K)	
N_2	5	3.68	92	3350
O_2	5	3.43	113	2273
H_2O	6	2.65	380	2295, 5255, 5400
Ar	3	3.42	124	–

Notations: R – radius of the bubble; dR/dt – bubble wall velocity; c – velocity of sound in bulk liquid medium; ρ_L – density of the liquid; ν – kinematic viscosity of liquid; σ – surface tension of liquid; λ – thermal conductivity of bubble contents; κ – thermal diffusivity of bubble contents; θ – characteristic vibrational temperature(s) of the species; N_w – number of water molecules in the bubble; N_p – number of pollutant molecules in the bubble; t – time, D_w – diffusion coefficient of water vapor; D_p – diffusion coefficient for pollutant; C_w – concentration of water molecules in the bubble; C_p – concentration of pollutant molecules in the bubble; C_{wR} – concentration of water molecules at the bubble wall or gas-liquid interface; C_{pR} – concentration of pollutant molecules at the bubble wall or gas-liquid interface; $l_{diff,w}$ – instantaneous diffusive penetration depth for water molecules; $l_{diff,p}$ – instantaneous diffusive penetration depth for pollutant molecules; Q – heat conducted across bubble wall; T – temperature of the bubble contents; T_o – ambient (or bulk liquid medium) temperature; k – Boltzmann constant; N_{Ar} – number of Ar molecules in the bubble; f_i – translational and rotational degrees of freedom; $C_{V,i}$ – heat capacity at constant volume; N_{tot} – total number of molecules (gas + vapor) in the bubble; h – van der Waal's hard core radius; P_o – ambient (bulk) pressure in liquid; P_A – pressure amplitude of ultrasound wave; f – frequency of ultrasound wave.

* Data taken from Toegel [50]; Hirschfelder et al. [47]; Reid et al. [59].

3.1. Numerical solution

The set of five ordinary differential equations (ODEs) given in Table 1A constitute complete formulation for the radial motion of cavitation bubble with associated heat and mass transfer effects. This set can be solved using Runge–Kutta fourth–fifth order adaptive step size method [51]. During the radial motion, the cavitation bubble may collapse at the instance of maximum compression, and its contents are released into the bulk medium. The word "collapse" essentially means fragmentation of the cavitation bubble. In a multi-bubble system, the radial motion of cavitation bubble is rather unstable and the fragmentation of the bubble can occur at the first compression after an initial expansion [8]. In view of this, the condition for the bubble collapse is taken to be first compression during radial motion.

The numerical solution of the bubble dynamics model requires 4 input physical parameters: (1) frequency and (2) pressure amplitude of ultrasound, (3) vapor pressure of water and pollutant, and (4) initial (or equilibrium) bubble radius. The values for these parameters have been determined as follows:

Acoustic frequency (f): The sonic processor used in the experiment produces an ultrasound wave with frequency of 20 kHz. This value is used for the simulations.

Acoustic pressure amplitude (P_A): The amplitude of the ultrasound wave generated by the sonicator probe, as calculated using a calorimetric method [15] was 150 kPa. However, due to the attenuation in the medium, the actual pressure amplitude sensed by the cavitation bubble located away from the probe tip is lesser than 150 kPa. A direct measurement of the local pressure amplitude in the vicinity of the cavitation bubble is not possible with the instrumentation used in the present study. Therefore, we assume about 15% attenuation of the ultrasound wave (as a *representative* value) in a saturated medium, and use a value of P_A = 125 kPa in the numerical simulations in this medium. For the degassed or unsaturated medium, the bubble population density is quite small, and hence, attenuation effect can be ignored. Therefore, we assume a value of P_A = 150 kPa for the simulations of radial motion of cavitation bubble in an unsaturated or degassed medium.

Vapor pressure of water and pollutant: The vapor pressure of water as well as pollutant at 25 °C was calculated with Antoine's equations [52]. The temperature of the bulk medium varied by about ±2 °C during sonication, as noted earlier. As the changes in vapor pressure with this fluctuation is very small (<10%), we have ignored the temperature fluctuation during simulations, assuming the bulk liquid medium at constant temperature of 25 °C. Vapor pressure of water reduces with the addition of salt. This reduction is accounted for using formulae given by Al-Shayji [53] for the simulations for salt-added medium.

Initial (or equilibrium) bubble radius (R_o): The bulk medium contains cavitation nuclei, which are tiny gas pockets trapped in the crevices of reactor or gas bubbles already suspended in the medium. Depending on the conditions of the medium, these nuclei may have a wide or narrow size range. It is rather difficult to estimate the exact size distribution of these cavitation nuclei. However, for an unsaturated medium, the size range of these nuclei is expected to be smaller than for the saturated medium. For simulations, one can use a representative size (which could be median of the size distribution) of R_o = 5 μm for an unsaturated medium, and R_o = 10 μm for the saturated medium.

3.2. Quantification of radical production

At the instance of maximum compression during radial motion, the temperature inside the bubble reaches extreme (~5000 K). In addition, due to an extremely small bubble volume, the concentration of the species is quite high. As a result of these two conditions, the rates of various reactions occurring in the bubble are very high. Therefore, we assume prevalence of thermodynamic equilibrium in the bubble [42,54], and estimate the equilibrium composition of the various species formed in the bubble with dissociation of entrapped water and pollutant molecules using software FACTSAGE. This software uses the free-energy minimization algorithm proposed by Eriksson [55]. A more rigorous approach in this regard would be to include various radical reactions in the mass balance equations along with heats of these reactions included in the energy balance [8,56]. Endothermicity of some of the radical reactions (for example, $H_2O \rightleftarrows H^{\cdot} + {}^{\cdot}OH$) works towards lowering of the peak temperature reached during transient bubble collapse. However, addition of this feature in the present model would change only the final quantitative answers, with trends remaining essentially unaltered.

4. Results

Due to extremely high unstability and reactivity, the reaction zone of the radicals generated from cavitation bubbles is restricted to only a small region in the vicinity of point of bubble collapse. These radicals do not diffuse to significant distance in the bulk liquid medium from location of collapse of bubble. Quite obviously, the hydroxylation reaction would occur only if a pollutant molecule is present in the reaction zone, where it can interact with the radicals. If the solution of pollutant is dilute, the probability of interaction between pollutant molecules and ·OH radicals becomes an important factor influencing the extent of degradation of the pollutant. On the other hand, the factor that determines the extent of degradation through pyrolysis route is the partial pressure of pollutant at the bubble–bulk interface. Following Raoult's law (for dilute solution of the pollutant), this depends on the vapor pressure of pollutant (in pure form) and the mole fraction of the pollutant at the bubble interface. Another factor that comes into picture is the hydrophobicity of the pollutant. Due to repulsive interactions between organic pollutant and water molecules, the pollutant molecules are "driven" towards the bubble interface [57,58], which also has a hydrophobic character. This results in enhanced concentration of pollutant molecules in the bubble–bulk interfacial region, which affects the degradation of the pollutant via both hydroxylation and pyrolysis routes. Due to higher concentration of pollutant at the bubble interface, the probability of radical–pollutant interaction increases, which favorably affects the degradation occurring through hydroxylation. Higher concentration at the bubble interface also raises the partial pressure of the pollutant that leads to higher evaporation and subsequent entrapment of the pollutant into the cavitation bubble, which undergoes pyrolytic decomposition at the extreme conditions reached during the transient collapse of the bubble.

The physical properties of the five pollutants are shown in Table 2A. These are essentially derivatives of benzene obtained with grafting of –OH, $–NO_2$ and –Cl groups. However, these groups impart different characteristics to the compounds. $–NO_2$ and –Cl groups impart strong hydrophobic character to the compound, while –OH group imparts strong hydrophilic character to the compound. If both groups are present, for example –OH and $–NO_2$ as in PNP and –OH and –Cl as in 2,4-DCP, the character of the compound is expected to be intermediate. On the basis of the properties listed in Table 2A, one can characterize various pollutants on *relative* basis as follows:

Ph: High solubility, high hydrophilicity and nonvolatile.

CB: Low solubility, high hydrophobicity and volatile.

PNP: High solubility, moderate hydrophilicity and nonvolatile.

NB: Moderate solubility, moderate hydrophobicity and nonvolatile.

Table 2A
Physico-chemical properties of various organic pollutants.

Properties	Phenol	Chlorobenzene	p-Nitrophenol	Nitrobenzene	2,4-Dichlorophenol
Water solubility at 25 °C (ppm)	83,000	500	16,000	1900	4500
Water–octanol partition coefficient (log K_{OW})	1.46	2.84	1.91	1.86	3.06
Vapor pressure at 25 °C (Pa)	46	1598	0.0032	33.69	25.84

Table 2B
Energies of various bonds present in the pollutants.

Sr. No.	Type of bond	Bond energy (kJ mol^{-1})
1.	C–O	1076.38 ± 0.67
2.	C–N	750.0 ± 2.9
3.	C–Cl	394.9 ± 13.4

2,4-DCP: Low solubility, high hydrophobicity and nonvolatile.

With this preamble, we analyze the results of degradation of five pollutants under different conditions by correlating them with the physico-chemical properties of the pollutants and the simulations of radial motion of cavitation bubble.

4.1. Experimental results

The percentage degradation of five pollutants under different conditions is depicted in Table 3. The salient features of the experimental results, i.e. influence of each of the experimental parameter on the extent of degradation of pollutants, are given below:

Initial pollutant concentration: This parameter was applied for the degradation of Ph and CB. The extent of degradation of both of these pollutants in saturated medium increased with increasing initial concentration.

Saturation level (or dissolved gas content) of the medium: Effect of this parameter was examined for three pollutants, viz. NB, PNP and 2,4-DCP. The degradation of NB and 2,4-DCP increased with reduced saturation level (or degassing) of the medium, while degradation of PNP was higher for saturated medium.

Gas bubbling (or sparging) through the medium: Influence of this parameter was assessed for Ph and 2,4-DCP. For both of these compounds, bubbling of nitrogen through the medium resulted in least degradation. However, the overall trend for four gases was different for the two compounds. For Ph, the trend in degradation was: O_2 > Air > Ar > N_2, while for 2,4-DCP the trend was: Air > Ar > O_2 > N_2.

Salt addition: This experimental parameter was applied for the degradation of all five pollutants. Degradation of Ph showed marked enhancement with salt addition for both 50 and 100 ppm initial concentration. Degradation of NB (in both saturated and unsaturated medium) and 2,4-DCP (in saturated medium) did not alter much, while degradation of PNP reduced slightly in both saturated and unsaturated medium with salt addition.

Addition of $FeSO_4 \cdot 7H_2O$: Effect of this parameter was investigated for three pollutants, viz. NB and PNP (in both saturated and unsaturated medium) and 2,4-DCP in saturated medium. For NB and 2,4-DCP, $FeSO_4 \cdot 7H_2O$ added solutions gave only slight improvement in degradation over pure solutions. On the contrary, PNP degradation showed marked (∼100%) enhancement with $FeSO_4$ addition.

4.2. Simulation results

Simulations of radial motion of 5 and 10 μm air bubbles and 10 μm argon bubble are given in Figs. 2–4, respectively. These simulations are representative of cavitation phenomena in dilute solutions of nonvolatile pollutants such as Ph, PNP, NB and 2,4-DCP. In these simulations, the evaporation of the pollutant into the bubble has been ignored for the reasons stated in previous section. Fig. 5 shows the special case of radial motion of 10 μm air bubble in CB solution of 50 ppm concentration. In this case, the evaporation of the pollutant has been taken into account as CB is a volatile pollutant. The summary of entire simulations results is given in Tables 4A–4C that lists the temperature and pressure peaks reached at the moment of transient collapse of cavitation bubble, the number of water and pollutant molecules entrapped in the bubble at the moment of collapse and the equilibrium composition of the various species resulting out of dissociation of entrapped molecules in the bubble at the conditions of temperature and pressure reached during transient collapse. Also listed in these tables is the net production of ·OH radicals (N_{OH}) per cavitation bubble. It could be seen that the trend in production of ·OH radical that is responsible for hydroxylation reaction varies as: Ar > Air > O_2 > N_2. The reasoning underlying this trend can be explained as follows:

1. Ar bubbles produce the highest number of radicals among all four gases. This is a consequence of the highest temperature peak reached at the collapse due to monatomic nature of Ar.

Table 3
Experimental results on degradation of various pollutants with different experimental techniques.

Experimental parameters		% Degradation of pollutants				
		Phenol	Chlorobenzene	Nitrobenzene**	p-Nitrophenol*	2,4-Dichlorophenol**
Initial concentration	50 ppm (saturated medium)	1.90 ± 0.14	65.86 ± 5.01	–	–	–
	100 ppm (saturated medium)	2.09 ± 0.08	65.59 ± 3.64	–	–	–
Dissolved gas content	Saturated medium	–	–	18.43 ± 0.61	4.22 ± 0.45	5.66 ± 0.66
	Unsaturated medium	–	–	31.80 ± 0.37	2.94 ± 0.25	8.68 ± 0.30
Salt addition (4% NaCl)	Saturated medium	6.23 ± 0.35 (50 ppm) 5.25 ± 0.13 (100 ppm)	70.22 ± 6.58 (50 ppm) 70.09 ± 2.21 (100 ppm)	20.31 ± 1.63	3.51 ± 0.04	4.98 ± 0.72
	Unsaturated medium	–	–	28.23 ± 5.24	2.79 ± 0.36	–
Gas bubbling (pure solution)	Nitrogen	1.39 ± 0.28	–	–	–	5.66 ± 0.20
	Argon	2.20 ± 0.49	–	–	–	6.92 ± 0.43
	Oxygen	4.09 ± 0.51	–	–	–	6.86 ± 0.90
	Air	2.53 ± 0.34	–	–	–	9.25 ± 0.04
$FeSO_4 \cdot 7H_2O$ addition (0.5 mM)	Saturated medium	–	–	22.94 ± 3.46	11.07 ± 0.25	5.73 ± 0.36
	Unsaturated medium	–	–	30.61 ± 2.70	4.31 ± 0.13	–

* For all experiments, the initial concentration of PNP was 10 ppm.
** For all experiments, the initial concentration of NB and 2,4-DCP was 100 ppm.

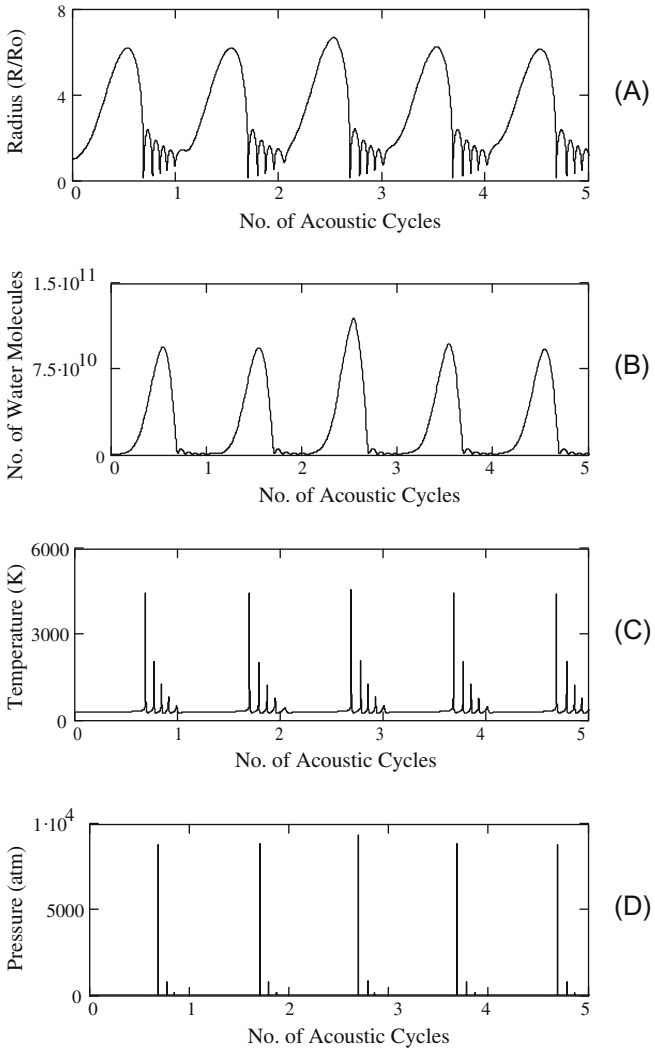

Fig. 2. Simulation of radial motion of 5 μm air bubble. Time variation of (A) normalized bubble radius (R/R_o); (B) number of water molecules in the bubble; (C) temperature of the bubble and (D) pressure inside the bubble.

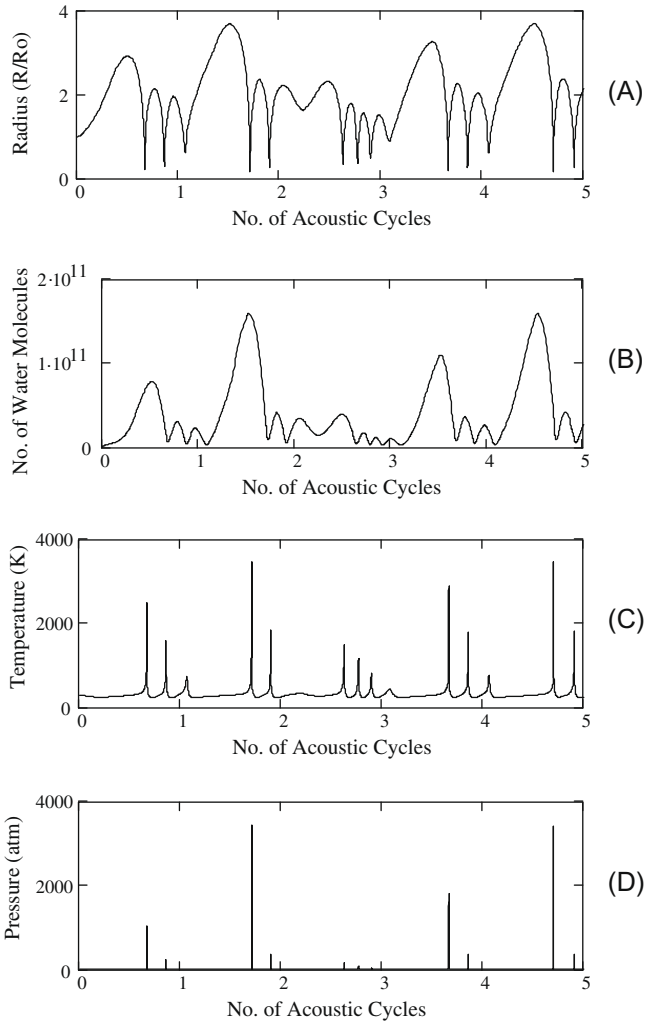

Fig. 3. Simulation of radial motion of 10 μm air bubble. Time variation of (A) normalized bubble radius (R/R_o); (B) number of water molecules in the bubble; (C) temperature of the bubble and (D) pressure inside the bubble.

2. The intensity of collapse of air, N_2 and O_2 bubbles is more-or-less the same, as indicated by the temperature peaks attained at the collapse of these bubbles. However, the equilibrium composition of the bubble varies due to scavenging of radicals by oxygen and nitrogen molecules present in the bubble.
3. For air bubble, the N_2 scavenges the H·, O· and ·OH radical to produce various species such as NO, N_2O, NO_2, HNO and HNO_2 through the following reactions [45]:

$$N_2 + O^{\cdot} \rightleftharpoons N^{\cdot} + NO \quad (R.1)$$

$$N_2 + {}^{\cdot}OH \rightleftharpoons N_2H + O^{\cdot} \quad (R.2)$$

$$N_2 + {}^{\cdot}OH \rightleftharpoons N_2O + H^{\cdot} \quad (R.3)$$

$$N_2 + {}^{\cdot}OH \rightleftharpoons NH + NO \quad (R.4)$$

$$N_2 + H^{\cdot} \rightleftharpoons N_2H \quad (R.5)$$

$$N_2 + H^{\cdot} \rightleftharpoons NH + N^{\cdot} \quad (R.6)$$

$$N + {}^{\cdot}OH \rightleftharpoons NO + H^{\cdot} \quad (R.7)$$

$$N_2O + O^{\cdot} \rightleftharpoons 2NO \quad (R.8)$$

$$NO + OH^{\cdot} \rightleftharpoons NO_2 \quad (R.9)$$

$$NH + {}^{\cdot}OH \rightleftharpoons NH_2 + O^{\cdot} \quad (R.10)$$

$$NH_2 + O^{\cdot} \rightleftharpoons H^{\cdot} + HNO \quad (R.11)$$

$$HNO + O^{\cdot} \rightleftharpoons NH + O_2 \quad (R.12)$$

$$HNO + O^{\cdot} \rightleftharpoons NO + {}^{\cdot}OH \quad (R.13)$$

$$HNO + {}^{\cdot}OH \rightleftharpoons NO + H_2O \quad (R.14)$$

However, O_2 reacts with these species to regenerate O· and ·OH radicals through the following reactions:

$$N + O_2 \rightleftharpoons NO + O^{\cdot} \quad (R.15)$$

$$NO + O_2 \rightleftharpoons NO_2 + O^{\cdot} \quad (R.16)$$

$$NH + O_2 \rightleftharpoons HNO + O^{\cdot} \quad (R.17)$$

$$NH + O_2 \rightleftharpoons NO + {}^{\cdot}OH \quad (R.18)$$

$$N_2 + O_2 \rightleftharpoons N_2O + O^{\cdot} \quad (R.19)$$

O· radicals also react with H· and ·OH radicals to produce $HO_2^{\cdot}$ radical as follows:

$$H^{\cdot} + O_2 \rightleftharpoons HO_2^{\cdot} \quad (R.20)$$

$${}^{\cdot}OH + O_2 \rightleftharpoons HO_2^{\cdot} + O^{\cdot} \quad (R.21)$$

4. For O_2 bubbles, the yield of H_2O_2 and O_3 is much higher than other bubbles due to extensive scavenging of O·, H· and ·OH radicals by the O_2 molecules through the reactions:

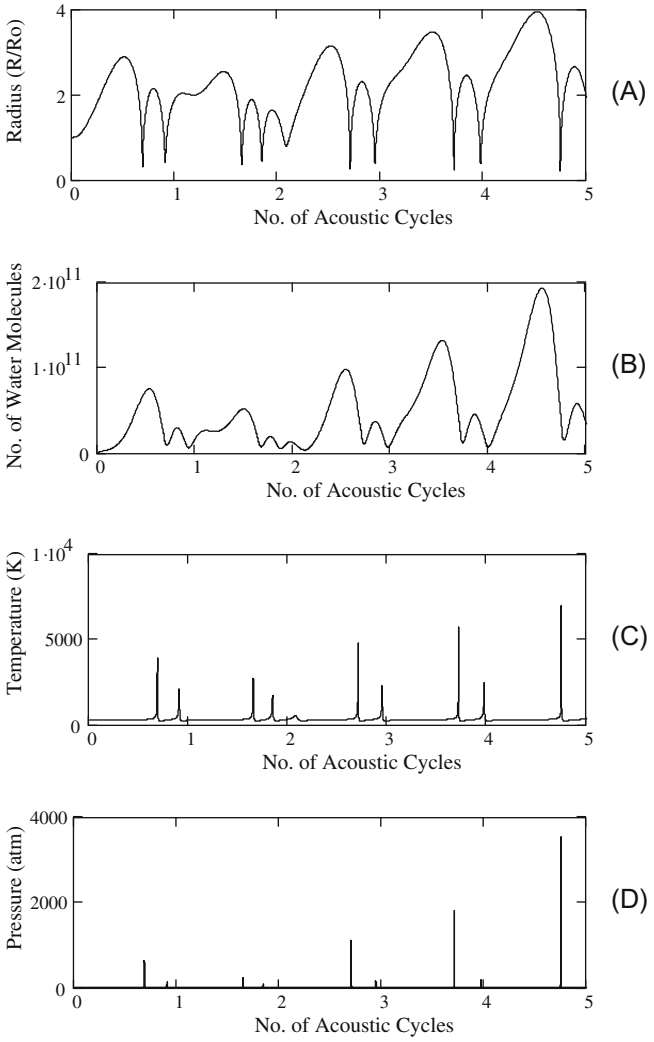

Fig. 4. Simulation of radial motion of 10 μm argon bubble. Time variation of (A) normalized bubble radius (R/R_o); (B) number of water molecules in the bubble; (C) temperature of the bubble and (D) pressure inside the bubble.

$$O^{\cdot} + O_2 \rightarrow O_3 \quad \text{(R.22)}$$

$$2HO_2^{\cdot} \rightleftharpoons H_2O_2 + O_2 \quad \text{(R.23)}$$

This results in loss of oxidation potential. The overall yield of radicals is thus reduced.

5. Production of radicals by N_2 bubbles is the least. This is a consequence of the extensive scavenging of the radical species by N_2 molecules (through reactions (R.1)–(R.14)). Secondly, there is no regeneration of $O^{\cdot}$ and $^{\cdot}OH$ radicals by O_2, as in case of air bubbles. The overall effect is massive loss of radicals that reduces the oxidation potential of these bubbles.

5. Discussion

In this section, we try to correlate the data in Table 2A–4C to deduce the physical features of sonochemical degradation of the aromatic pollutants. Prior to this, we briefly outline as how the various experimental parameters used in the degradation studies alter characteristics of the cavitation phenomena in the system, and hence, the extent of degradation of the pollutants.

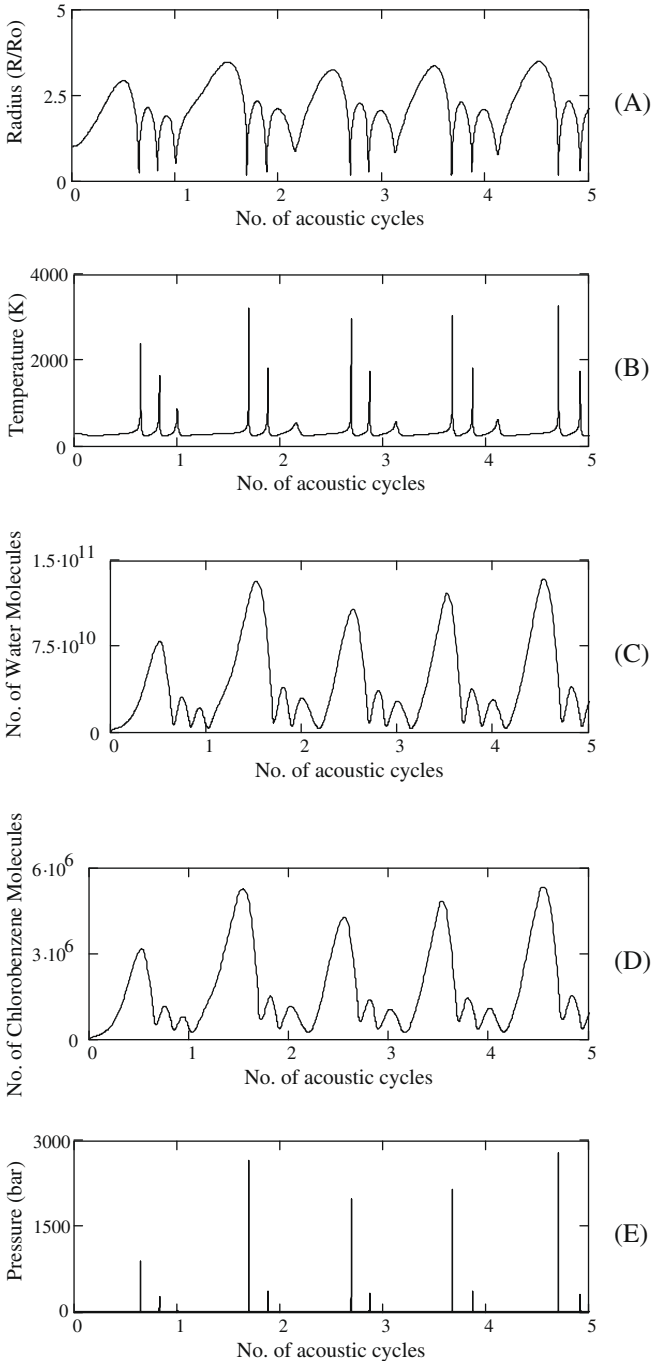

Fig. 5. Simulation of the radial motion of 10 μm air bubble in 50 ppm chlorobenzene solution. Time variation of (A) normalized bubble radius (R/R_o); (B) temperature in the bubble; (C) number of water molecules in the bubble; (D) number of chlorobenzene molecules in the bubble and (E) pressure inside the bubble.

Initial concentration: Rise in the initial concentration of pollutant has two implications: first, rise in the probability of radical–pollutant interaction, and secondly, rise in the interfacial concentration of the pollutant due to which the extent of evaporation of the pollutant into the cavitation bubble increases. This enhances the degradation through pyrolytic route.

Dissolved gas concentration: This factor affects the extent of radical production in the medium by altering the intensity of the transient collapse of the bubble via rectified diffusion. In a saturated medium, the dissolved gas slowly diffuses into the

Table 4A
Summary of the simulation results for argon, nitrogen and oxygen bubbles in aqueous solutions of phenol, nitrobenzene, *p*-nitrophenol and 2,4-dichlorophenol.

Species	Parameters for simulations		
	Argon bubble R_o = 10 μm	Nitrogen bubble R_o = 10 μm	Oxygen bubble R_o = 10 μm
	Conditions at the first collapse of the bubble		
	T_{max} = 3937 K P_{max} = 628.7 bar $N_{Ar} = 1.178 \times 10^{+11}$ $N_{WT} = 1.51 \times 10^{+10}$	T_{max} = 2397 K P_{max} = 1407 bar $N_{N_2} = 1.178 \times 10^{+11}$ $N_{WT} = 1.48 \times 10^{+10}$	T_{max} = 2303 K P_{max} = 1539 bar $N_{O_2} = 1.178 \times 10^{+11}$ $N_{WT} = 1.47 \times 10^{+10}$
Equilibrium composition of bubble contents at transient collapse			
H_2O	6.587×10^{-1}	1.109×10^{-1}	1.099×10^{-1}
H_2	1.314×10^{-1}	9.211×10^{-4}	6.251×10^{-6}
OH	1.145×10^{-1}	2.838×10^{-4}	1.809×10^{-3}
H	3.888×10^{-2}	1.262×10^{-5}	6.232×10^{-7}
O_2	3.686×10^{-2}	1.279×10^{-4}	8.879×10^{-1}
O	1.899×10^{-2}	2.557×10^{-6}	1.206×10^{-4}
HO_2	5.463×10^{-4}	4.626×10^{-7}	2.778×10^{-4}
H_2O_2	7.150×10^{-5}	2.613×10^{-7}	1.808×10^{-5}
O_3	3.655×10^{-7}	0	5.395×10^{-6}
N_2	0	8.873×10^{-1}	0
NO	0	5.244×10^{-4}	0
N_2O	0	1.045×10^{-6}	0
NH_3	0	4.506×10^{-7}	0
NO_2	0	4.429×10^{-7}	0
HNO	0	2.584×10^{-7}	0
HNO_2	0	2.978×10^{-7}	0
NH_2	0	1.995×10^{-8}	0
N_{OH}	1.728×10^{9}	3.763×10^{7}	2.397×10^{8}

Notations for Table 4: T_{max} – temperature peak reached in the bubble at the time of first collapse; P_{max} – pressure peak reached in the bubble at the time of first collapse; N_{WT} – number of water molecules trapped in the bubble at the instance of first collapse; N_{N_2} – number of oxygen molecules in the bubble (for air and oxygen bubbles); N_{OH} – number of ·OH radicals produced per cavitation bubble.

Table 4B
Summary of the simulation results for variation in the saturation level of the medium for nitrobenzene, *p*-nitrophenol and 2,4-dichlorophenol solutions.

Species	Parameters for simulations	
	Air bubble R_o = 5 μm	Air bubble R_o = 10 μm
	Conditions at first compression of the bubble	
	T_{max} = 4426 K P_{max} = 8812 bar $N_{N_2} = 1.271 \times 10^{+10}$ $N_{O_2} = 3.379 \times 10^{+9}$ $N_{WT} = 2.70 \times 10^{+9}$	T_{max} = 2478 K P_{max} = 1044 bar $N_{N_2} = 9.305 \times 10^{+10}$ $N_{O_2} = 2.474 \times 10^{+10}$ $N_{WT} = 1.09 \times 10^{+10}$
Equilibrium composition of bubble contents at transient collapse		
N_2	7.085×10^{-1}	7.122×10^{-1}
O_2	1.335×10^{-1}	1.805×10^{-1}
NO	1.188×10^{-1}	2.047×10^{-2}
H_2O	9.797×10^{-3}	8.379×10^{-2}
OH	1.242×10^{-2}	2.126×10^{-3}
O	1.214×10^{-2}	1.697×10^{-4}
NO_2	2.182×10^{-3}	5.093×10^{-4}
HO_2	7.135×10^{-4}	1.054×10^{-4}
H_2	3.419×10^{-4}	3.254×10^{-5}
N_2O	5.862×10^{-4}	3.151×10^{-5}
H	6.106×10^{-4}	4.006×10^{-6}
HNO_2	2.053×10^{-4}	4.659×10^{-5}
HNO	1.048×10^{-4}	1.651×10^{-6}
H_2O_2	1.972×10^{-5}	7.629×10^{-6}
O_3	2.914×10^{-5}	6.983×10^{-7}
N	6.444×10^{-5}	0
HNO_3	7.662×10^{-7}	1.791×10^{-7}
NO_3	1.368×10^{-6}	3.999×10^{-8}
NH	6.321×10^{-6}	0
N_2O_3	8.790×10^{-7}	0
NH_2	1.198×10^{-6}	0
NH_3	1.822×10^{-7}	0
N_3	1.333×10^{-6}	0
N_{OH}	2.334×10^{8}	2.736×10^{8}

Note: Air bubble of 10 μm size represents saturated medium while air bubble of 5 μm size represents unsaturated medium.

Table 4C
Summary of the simulation results for air bubbles in chlorobenzene solution.

Species	Parameters for simulation	
	50 ppm solution	100 ppm solution
	Conditions at the first compression of the bubble	
	T_{max} = 2383 K P_{max} = 888.2 bar $N_{cb} = 8.1 \times 10^5$ $N_w = 1.0502 \times 10^{10}$	T_{max} = 2383 K P_{max} = 888.2 bar $N_{Cb} = 8.1 \times 10^5$ $N_w = 1.0502 \times 10^{10}$
Equilibrium composition of bubble contents at transient collapse		
O_2	6.994×10^{-1}	6.994×10^{-1}
H_2O	2.955×10^{-1}	2.955×10^{-1}
OH	4.262×10^{-3}	4.262×10^{-3}
O	2.207×10^{-4}	2.207×10^{-4}
HOO	4.127×10^{-4}	4.127×10^{-4}
CO_2	1.375×10^{-4}	1.375×10^{-4}
H_2	3.879×10^{-5}	3.879×10^{-5}
H_2O_2	3.963×10^{-5}	3.963×10^{-5}
HCl	2.113×10^{-5}	2.113×10^{-5}
O_3	3.702×10^{-6}	3.702×10^{-6}
H	3.049×10^{-6}	3.049×10^{-6}
Cl	1.182×10^{-6}	1.182×10^{-6}
ClO	3.504×10^{-7}	3.504×10^{-7}
CO	1.035×10^{-7}	1.035×10^{-7}
HOCl	2.675×10^{-7}	2.675×10^{-7}
ClO_2	1.233×10^{-9}	1.233×10^{-9}
Cl_2	1.972×10^{-10}	1.972×10^{-10}

Note: In these simulations the evaporation of the pollutant into the cavitation bubble has been taken into account.

cavitation bubble during oscillations, as result of which the equilibrium of the bubble grows. This gas cushions the transient collapse of the bubble, and thus, the temperature and pressure peaks attained in the bubble reduce, resulting in the reduction of ·OH radical production. On the other hand, in an unsaturated medium gas inside the bubble dissolves into the medium during oscillations with consequent rise in the intensity of collapse and radical production.

Salt addition: Addition of salt to the medium increases the ionic strength of the medium. This enhances the hydrophobic repulsive interactions between pollutant and water molecules. Due to this, the pollutant molecules are "pushed" towards the bubble interface causing increased concentration of pollutant molecules. This phenomenon boosts the probability of radical–pollutant interaction as well as extent of evaporation of pollutant into the bubble due to rise in the partial pressure of the pollutant at the bubble interface. Thus, salt addition causes increase in degradation through both hydroxylation and pyrolysis routes.

Gas bubbling or sparging: This technique is used to seed external cavitation nuclei in the medium made up of desired gas. The basis for this technique is that different monatomic and diatomic gases show different cavitation behavior. Monatomic gas such as Ar, by virtue of its low heat capacity, heats up the cavitation bubble to far higher temperatures than diatomic gases like N_2, air and O_2. On the other hand, presence of O_2 molecules in the air and O_2 bubbles gives rise to scavenging of radicals (i.e. conservation of radicals due to reaction of oxygen with other species to generate new radical species) that influences the composition of the bubble at transient collapse. In addition, during bubbling of air or O_2 through the liquid medium, O_2 also continuously dissolves in the medium, as a result of which the concentration of dissolved O_2 (DO) is maintained at saturation level. DO gives rise to scavenging effect in the bulk liquid medium, due to which the penetration

depth of radicals (or the "reaction zone" of radicals) from location of bubble collapse increases. This has a favorable effect on degradation in that it increases the probability of radical–pollutant interaction.

$FeSO_4$ addition: Addition of Fe^{2+} ions in the medium gives rise to Fenton's reagent type action. In case of dilute solutions of pollutants, the probability of radical–pollutant interaction is low, as a result of which a large fraction of radicals undergo recombination. This is a loss of oxidation potential. The predominant radical species generated by transient collapse of bubble is ·OH, and hence, the principal product formed out of radical recombination is H_2O_2. Fe^{2+} reacts with H_2O_2 to generate ·OH radicals according to following reactions:

$$\cdot OH + \cdot OH \rightleftharpoons H_2O_2 \quad (R.24)$$

$$H_2O_2 + Fe^{2+} \rightarrow Fe^{3+} + OH^- + \cdot OH \quad (R.25)$$

$$Fe^{3+} + H_2O_2 \rightarrow Fe^{2+} + HO_2^{\cdot} + H^+ \quad (R.26)$$

$$Fe^{3+} + HO_2^{\cdot} \rightarrow Fe^{2+} + O_2 + H^+ \quad (R.27)$$

This Fenton's type action not only reverts the oxidation potential loss, but also helps in deeper penetration of the radical action from the location of bubble collapse, which increases the probability of radical–pollutant interaction.

On the basis of above discussion, we try to establish the physical mechanism of the degradation of each pollutant and also attempt to link it with the physico-chemical characteristics of the pollutant. Moreover, we compare the extent of degradation of pollutants under same experimental condition, and try to link it with their physico-chemical characteristics.

(1) Due to nonvolatile nature, Ph is not expected to evaporate into the bubble, and hence, the degradation mechanism of Ph is expected to be hydroxylation. The highest degradation of Ph in presence of O_2 indicates that the degradation occurs in the bulk medium via hydroxylation. This is further corroborated by enhancement in degradation observed with salt addition and increasing initial concentration.

(2) Due to volatile and hydrophobic nature, CB is expected to evaporate into the bubble and undergo pyrolytic decomposition. This mode is expected to cause very rapid degradation. CB has the highest degradation rate among all pollutants, which is one order of magnitude higher than any other pollutant. Marginal effect of salt addition on the degradation rate is attributed to hydrophobic nature of CB, as a result of which its concentration in the bubble–bulk interfacial region is near or at saturation. The extent of degradation increases with initial concentration, and this is attributed to higher evaporation of CB into the bubble at higher initial concentrations.

(3) Due to nonvolatile nature of NB, it is not expected to evaporate into the bubble, and moreover, due to moderate hydrophobicity its concentration in the interfacial region is higher than in the bulk. Significant rise in degradation of NB with unsaturation of the medium indicates hydroxylation as the predominant mechanism of degradation. Neither salt addition nor $FeSO_4$ addition creates any significant change in degradation indicates that hydrophobic interactions and radical scavenging is unimportant for NB degradation. This is attributed to the hydrophobicity of NB, due to which the concentration of NB at bubble interface is near or at saturation, and hence, does not change with salt addition. As a result, most of the degradation occurs in the bubble–bulk interfacial region with maximum probability of radical–pollutant interaction. Perceptibly, addition of radical scavenger like Fe^{2+} also does not make a significant difference to the extent of degradation.

(4) PNP has nonvolatile and moderately hydrophilic character. However, the chemistry of its degradation is different from other pollutants (Kotronarou et al. [27]). It initially undergoes thermal decomposition with the cleavage of C–N bond in the boundary layer surrounding the bubble that gets heated up during collapse, followed by hydroxylation in the bulk medium. Moreover, due to very low concentration (10 ppm) used in the experiments, the factor of radical scavenging becomes crucially important in the overall degradation. Reduction in the degradation of PNP is attributed to the reduction in the thickness of the thermal boundary layer, where it undergoes decomposition prior to hydroxylation. Reduction in the degradation with salt addition is attributed to reduction in the DO content, due to which the scavenging action reduces. The importance of the scavenging action in the bulk medium is further corroborated by sharp rise in the degradation with the addition of Fe^{2+}. All of these results point at hydroxylation in the bulk medium as the predominant degradation mechanism.

(5) 2,4-DCP is characterized by nonvolatile and hydrophobic nature. Sharp rise in degradation with unsaturation of the medium indicates hydroxylation at the bubble–bulk interfacial region as the predominant degradation pathway. Moreover, due to low solubility (4500 ppm), the concentration at the bubble–bulk interface is small, although the interfacial region is expected to be near or at saturation due to hydrophobic nature of the pollutant. The scavenging action in the interfacial region, thus, becomes an important factor in degradation. These arguments are supported by the highest degradation observed in the presence of air. Relatively low degradation rates with Fe^{2+} addition in comparison to air or O_2 sparging indicate that scavenging action in the bulk medium is unimportant. Interpreting these outcomes in other way provides corroboration that the predominant region of degradation is the bubble–bulk interfacial region.

The above inferences are summarized in Table 5 that lists the predominant mechanism and the location of degradation for the five pollutants.

Table 5
Predominant mechanism and location of degradation of various organic pollutants.

Sr. No.	Pollutant	Mechanism of degradation	Location of degradation
1	Phenol	Hydroxylation	Bulk medium
2	Chlorobenzene	Pyrolytic decomposition	Inside the cavitation bubble
3	Nitrobenzene	Hydroxylation	Bubble–bulk interfacial region
4	p-Nitrophenol	Thermal decomposition followed by hydroxylation	Bubble–bulk interfacial region (thermal decomposition) Bulk medium (hydroxylation)
5	2,4-Dichlorophenol	Hydroxylation	Bubble–bulk interfacial region

5.1. Comparative analysis

We now try to contrast the trends in degradation rates of different pollutant under same experimental conditions, and try to explain them on the basis of similarities/differences in the physicochemical properties of the pollutants. Before we proceed, we would like to note that degradation would essentially mean breakage of bond, and hence, we list in Table 2B the energies for C–Cl, C–O and C–N bonds present in the pollutants under consideration. An underlying supposition in this approach is that the degradation would essentially commence with the breakage the external bond, i.e. bond between C atom of the aromatic ring and the external group attached, as the aromatic ring itself is a highly stable structure. The higher the energy of the bond(s) present in the molecule, the more arduous the degradation of the pollutant. In view of different bond energies and chemical composition of the pollutant, we can rank the pollutants in the following order for stability or resistance towards degradation: Ph > PNP > 2,4-DCP > NB > CB.

- Increasing initial concentration raised the percentage degradation of both Ph and CB. However, the extent of degradation of CB was one order of magnitude than that of Ph. This is clearly attributed to the difference in the mode of degradation. Due to volatile nature CB evaporates into the bubble and undergoes complete thermal decomposition. On the other hand, Ph being nonvolatile is degraded by reaction with ·OH radicals in the bulk medium. This mode of degradation has lesser efficiency due to low probability of ·OH radical and pollutant interaction in a dilute solution. In addition, the C–O bond present in Ph has the highest energy, which makes Ph highly resistant towards degradation. Nonetheless, one can perceive that increasing initial concentration raises both evaporation into the bubble as well as probability of ·OH radical interaction, and hence, we see similar trends in degradation of Ph and CB with this parameter.
- With reduction in the dissolved gas content (or unsaturation of the medium), degradation of NB and 2,4-DCP shows a similar (i.e. increasing) trend, while degradation of PNP shows an opposite (i.e. decreasing) trend. However, the extent of degradation of NB is much higher than that of 2,4-DCP. Again, this is attributed to the mode of degradation of these compounds. Both NB and 2,4-DCP are degraded by hydroxylation in the bubble–bulk interfacial region, while PNP degradation occurs by thermal decomposition in the thermal boundary layer around the bubble, followed by the hydroxylation in the bulk medium. Reduction in the dissolved gas content of the medium increases the extent of ·OH radical production from cavitation bubbles, as a result of which degradation of both NB and 2,4-DCP increases. On the other hand, the thickness of the thermal boundary layer reduces with degassing of the medium, and hence, the extent of PNP degradation. Higher percentage degradation of NB than 2,4-DCP (although the mode and location of degradation being same) can be explained on the basis of lesser energy of the C–N bond (present in NB) than the energies of the C–O and C–Cl bonds present in 2,4-DCP.
- Addition of salt to the medium shows different trends: Ph degradation rises sharply; degradation of NB, 2,4-DCP and CB stays almost same, while degradation of PNP reduces. As noted earlier, salt addition increases the ionic strength of the medium, and hence, the hydrophobic interactions between pollutant and water molecules. The pollutant molecules are then driven towards the bubble–bulk interfacial region. This boosts the probability of the radical–pollutant interaction as well as the extent of evaporation of pollutant in the bubble. Thus, the extent of degradation of pollutants undergoing degradation by both pyrolysis and hydroxylation route is expected to enhance with salt addition. However, this effect is marked only for the pollutants with hydrophilic character, such as Ph and PNP. If the pollutant has already a strong hydrophobic character, its concentration at the bubble–bulk interfacial region is already at saturation, and hence, does not change with salt addition. This is the case of NB, CB and 2,4-DCP. Despite different modes of degradation, these pollutants show similar trend in degradation with salt addition. Once again, we see that the percentage degradation is the highest for CB followed by NB and 2,4-DCP – in that order. This is attributed to both mode of degradation (pyrolysis for CB and hydroxylation for NB and 2,4-DCP) and the bond energies (C–Cl bond in CB, C–N bond in NB and C–Cl and C–O bonds in 2,4-DCP). Reduction in PNP degradation with salt addition is an anomaly. We explain this on the basis of reduction in dissolved O_2 (DO) content of the medium with salt addition, which reduces the scavenging action. Due to very low (10 ppm) concentration, scavenging action (in both bulk and interfacial region) plays a crucial role in degradation of PNP. Lessening of radical scavenging with salt addition results in reduction of the percentage degradation.
- Sparging of different gases through the medium shows different trends for Ph and 2,4-DCP. For Ph, highest degradation is seen for oxygen sparging while 2,4-DCP gives highest degradation for air sparging. In addition, percentage degradation of 2,4-DCP is significantly higher than that of Ph. We attribute these results to the hydrophobic and hydrophilic nature of 2,4-DCP and Ph, respectively, as a result of which the predominant location of degradation changes – although the mechanism of degradation, i.e. hydroxylation, stays the same. Due to hydrophobic nature, the bubble–bulk interfacial region is always saturated with 2,4-DCP. Thus, the probability of radical–pollutant interaction is maximum and 2,4-DCP predominantly degrades in interfacial region. As air bubble produces more radicals than O_2 bubble, the degradation of 2,4-DCP is higher for air bubbles. On the contrary, phenol being hydrophilic stays in the bulk medium and degradation occurs in the bulk medium. Thus, the probability of radical–pollutant interaction is dominated by the scavenging (and not production) of radicals, which is expected to be higher for O_2-sparged solution than air. Thus, although air bubbles produce more radicals than O_2, the net utilization of radicals (and hence extent of degradation) is higher for O_2-sparged solution. The predominant reaction zone of radicals is the bubble–bulk interfacial region. As noted earlier, due to highly unstable nature, the most of the radicals react in the close neighbourhood of the location of collapse of the bubble. Although, the scavenging action helps in expansion of this zone with deeper penetration of radicals, its effect is marginal. Due to hydrophobic nature of 2,4-DCP its concentration in the bubble–bulk interfacial region is high that results in higher radical interaction and higher degradation. Conversely, the probability of radical–pollutant interaction, even in presence of scavenging effect, is low for Ph that preferentially stays in the bulk medium. Thus, the extent of degradation is much less for Ph than 2,4-DCP.
- Addition of $FeSO_4$ in the medium causes insignificant rise in the extent of degradation of NB (in both saturated and unsaturated media) and 2,4-DCP (in saturated medium). The degradation of PNP, nonetheless, shows a marked rise with $FeSO_4$ addition. This rise is more pronounced for saturated medium. As noted earlier, $FeSO_4$ addition basically results in radical scavenging (or conservation) through Fenton type action, which results in reversal of oxidation potential loss through radical recombination. As Fe^{2+} has ionic character, the scavenging action of Fe^{2+} is restricted to the bulk medium. Minor rise in degradation of nitrobenzene and 2,4-DCP with Fe^{2+} addition is attributed to the location of degradation. As mentioned in Table 5, these compounds are

predominantly degraded in the bubble–bulk interfacial region due to their hydrophobic character. Therefore, scavenging action of Fe^{2+} that mainly occurs in the bulk medium has very little influence on the degradation of these pollutants. In contrast, PNP being moderately hydrophilic essentially degrades in the bulk medium after undergoing thermal decomposition in the thermal boundary layer. As the concentration of PNP was very dilute, radical scavenging plays a crucial role in degradation of PNP. It is for these reasons that the degradation of PNP shows marked enhancement with $FeSO_4$ addition. If the medium is unsaturated, the thickness of the thermal boundary layer surrounding the bubble (where thermal decomposition of PNP occurs prior to hydroxylation) decreases. This phenomenon has an opposite and adverse effect on degradation, and it reduces the prominence of the favourable action of radical scavenging by $FeSO_4$. Thus, rise in overall degradation of PNP is restricted in the unsaturated medium.

6. Conclusions

In this paper, we made a simultaneous study of the trends in sonochemical degradation of five organic pollutants with widely differing physico-chemical properties under similar experimental conditions. The experimental conditions (or parameters) employed in this work essentially affected the sonochemical phenomena (production, conservation and utilization of ·OH radicals) in the liquid medium. We also made use of the simulations of radial motion of cavitation bubble and the radical production from it under different experimental conditions. Our analysis gave a vivid picture as how the sonochemical degradation behavior is a function of the physico-chemical properties of the pollutants such as solubility, hydrophobicity (represented by octanol/water partition coefficient) and vapor pressure. Simultaneous analysis of the experimental and simulation results could explain the similarities and dissimilarities between the trends in degradation as well as differences in the extent of percentage degradation of the five pollutants under similar experimental conditions. Briefly, we have tried to couple the chemistry of sonochemical degradation and physics of cavitation phenomenon of five most common pollutants found in industrial wastewater. This analysis not only gives a clear idea of the mechanistic aspects of degradation (i.e. the location and predominant mode of sonochemical degradation), but also gives the relative importance of radical production and scavenging (or conservation) in the overall process.

The analysis presented in this paper also helps in devising a general framework with which one can predict the physical or mechanistic features of sonochemical degradation of any other pollutant. We believe that any other pollutant with similar physico-chemical properties as those studied this paper would give similar sonochemical degradation behavior. For example, the mechanistic features of degradation of CCl_4 or other halobenzenes (such as bromobenzene) would resemble with that of CB, while mechanistic features of o-, m- and p-cresol degradation are expected to resemble with that of Ph. Sonochemical degradation of aniline, on the other hand, is expected to have similar mechanistic features as NB.

Acknowledgments

Authors gratefully acknowledge stimulating discussions with Prof. Franz Grieser and Dr. M. Ashokkumar (University of Melbourne, Australia) and Prof. A.B. Pandit and Dr. P.S. Bapat (UICT, Mumbai, India) regarding behavior of an organic solute at bubble–bulk interfacial region. Authors also thank Prof. Andrea Prosperetti (Johns Hopkins University), Dr. Brian Storey (Olin College of Engineering, Boston) and Dr. Rudiger Toegel (University of Twente, Netherlands) for their help in the bubble dynamics modeling. This work was financially supported by Department of Science and Technology (DST), Government of India under Fast Track Scheme for Young Scientists.

References

[1] R. Andreozzi, V. Caprio, A. Insola, R. Marotta, Catal. Today 53 (1999) 51.
[2] P.R. Gogate, A.B. Pandit, Adv. Environ. Res. 8 (2004) 501.
[3] P.R. Gogate, A.B. Pandit, Adv. Environ. Res. 8 (2004) 55.
[4] Y.G. Adewuyi, Ind. Eng. Chem. Res. 40 (2001) 4681.
[5] Y.G. Adewuyi, Environ. Sci. Technol. 39 (2005) 3409.
[6] A.J. Colussi, L.K. Weavers, M.R. Hoffmann, J. Phys. Chem. A 102 (35) (1998) 6927.
[7] K. Yasui, Phys. Rev. E 56 (1997) 6750.
[8] B.D. Storey, A.J. Szeri, Proc. R. Soc. Lond. Ser. A 456 (2000) 1685.
[9] K.S. Suslick, Science 247 (1990) 1439.
[10] E.J. Hart, A. Henglein, J. Phys. Chem. 89 (20) (1985) 4342.
[11] E.J. Hart, A. Henglein, J. Phys. Chem. 91 (13) (1987) 3654.
[12] L.K. Weavers, M.R. Hoffmann, Environ. Sci. Technol. 32 (1998) 3941.
[13] T.M. Lesko, Chemical Effects of Acoustic Cavitation, Ph.D. Thesis, California Institute of Technology, Pasadena, 2004.
[14] I. Hua, R.H. Hochemer, M.R. Hoffmann, Environ. Sci. Technol. 29 (1995) 2790.
[15] T. Sivasankar, A.W. Paunikar, V.S. Moholkar, AIChE J. 53 (5) (2007) 1132.
[16] J. Berlan, F. Trabelsi, H. Delmas, A.M. Wilhelm, J.F. Petrignani, Ultrason. Sonochem. 1 (2) (1994) S97.
[17] N. Serpone, R. Terzian, P. Colarusso, Res. Chem. Intermediates 18 (2–3) (1992) 183.
[18] C. Petrier, A. Francony, Ultrason. Sonochem. 4 (4) (1997) 295.
[19] C. Petrier, A. Francony, Water Sci. Technol. 35 (4) (1997) 175.
[20] W. Zheng, M. Michelle, M.A. Tarr, Ultrason. Sonochem. 12 (4) (2005) 313.
[21] D. Drijvers, H.V. Langenhove, K. Vervaet, Ultrason. Sonochem. 5 (1998) 13.
[22] D. Drijvers, H.V. Langenhove, V. Herrygers, Ultrason. Sonochem. 7 (2000) 87.
[23] Y. Jiang, C. Petrier, T. David Waite, Ultrason. Sonochem. 9 (3) (2002) 163.
[24] C. Petrier, Y. Jiang, M.-F. Lamy, Environ. Sci. Technol. 32 (1998) 1316.
[25] L.K. Weavers, F.H. Ling, M.R. Hoffmann, Environ. Sci. Technol. 32 (1998) 2727.
[26] D.M. Cropek, P.A. Kemme, Sonolysis of Nitroaromatic Compounds: 1,3-Dinitrobenzene and Nitrobenzene, USACERL Technical Report 99/13, 1998.
[27] A. Kotronarou, G. Mills, M.R. Hoffmann, J. Phys. Chem. 95 (9) (1991) 3630.
[28] M.R. Hoffmann, I. Hua, R. Hochemer, Ultrason. Sonochem. 3 (1996) S163.
[29] S. Goskonda, W.J. Catallo, T. Junk, Waste Manage. 22 (2002) 351.
[30] Y. Yasman, V. Bulatov, V.V. Gridin, S. Agur, N. Galil, R. Armon, I. Schechter, Ultrason. Sonochem. 11 (2004) 365.
[31] L. Wu, A. Li, G. Gao, Z. Fei, S. Xu, Q. Zhang, J. Mol. Catal. A: Chem. 269 (2007) 183.
[32] V.I. Ilyichev, V.L. Koretz, N.P. Melnokov, Ultrasonics 27 (1989) 357.
[33] D.V. Prasad Naidu, R. Rajan, R. Kumar, K.S. Gandhi, V.H. Arakeri, S. Chandrasekaran, Chem. Eng. Sci. 49 (6) (1994) 877.
[34] R. Rajan, R. Kumar, K.S. Gandhi, Chem. Eng. Sci. 53 (1998) 255.
[35] B.D. Storey, A.J. Szeri, Proc. R. Soc. Lond. Ser. A 457 (2001) 1685.
[36] V. Kamath, A. Prosperetti, F.N. Egolfopoulos, J. Acoust. Soc. Am. 94 (1993) 248.
[37] S. Sochard, A.M. Wilhelm, H. Delmas, Ultrason. Sonochem. 4 (1997) 77.
[38] C. Gong, D.P. Hart, J. Acoust. Soc. Am. 104 (1998) 2675.
[39] A.J. Colussi, M.R. Hoffmann, J. Phys. Chem. A 103 (1999) 11336.
[40] W.C. Moss, D.A. Young, J.A. Harte, J.L. Levalin, B.F. Rozsnyai, G.B. Zimmerman, I.H. Zimmerman, Phys. Rev. E 59 (1999) 2956.
[41] R. Toegel, B. Gompf, R. Pecha, D. Lohse, Phys. Rev. Lett. 85 (2000) 3165.
[42] S.J. Krishnan, P. Dwivedi, V.S. Moholkar, Ind. Eng. Chem. Res. 45 (2006) 1493.
[43] K.S. Kumar, V.S. Moholkar, Chem. Eng. Sci. 62 (2007) 2698.
[44] J.B. Keller, M. Miksis, J. Acoust. Soc. Am. 68 (1980) 628.
[45] A. Prosperetti, A. Lezzi, J. Fluid Mech. 168 (1986) 457.
[46] C.E. Brennen, Cavitation and Bubble Dynamics, Oxford University Press, Oxford, 1995.
[47] J.O. Hirschfelder, C.F. Curtiss, R.B. Bird, Molecular Theory of Gases and Liquids, Wiley, New York, 1954.
[48] E.U. Condon, H. Odishaw, Handbook of Physics, McGraw Hill, New York, 1958.
[49] R.B. Bird, W.E. Stewart, E.N. Lightfoot, Transport Phenomena, second ed., Wiley, New York, 2001.
[50] R. Toegel, Reaction–Diffusion Kinetics of a Single Sonoluminescing Bubble, Ph.D. Dissertation, Twente University Press, Enschede, 2002.
[51] W.H. Press, S.A. Teukolsky, B.P. Flannery, W.T. Vetterling, Numerical Recipes, second ed., Cambridge University Press, New York, 1992.
[52] NIST Data Gateway, Chemistry Webbook, 2001, <http://webbook.nist.gov/chemistry>.
[53] K.A. Al-Shayji, Modeling, Simulation and Optimization of Large Scale Commercial Desalination Plants, Ph.D. Thesis, Virginia Polytechnique Institute and State University, Blacksburg, 1998.

[54] M. Brenner, S. Hilgenfeldt, D. Lohse, Rev. Mod. Phys. 74 (2002) 425.
[55] G. Eriksson, Chem. Scripta 8 (1975) 100.
[56] R. Toegel, D. Lohse, J. Chem. Phys. 118 (4) (2003) 1863.
[57] J. Seymour, R.B. Gupta, Ind. Eng. Chem. Res. 36 (9) (1997) 3453.
[58] P.S. Bapat, P.R. Gogate, A.B. Pandit, Ultrason. Sonochem. 14 (1) (2007) 564.
[59] R.C. Reid, J.M. Prausnitz, B.E. Poling, Properties of Gases and Liquids, McGraw Hill, New York, 1987.